Strain maps of the left atrium imaged with a novel high-resolution CINE MRI protocol*

Marta Varela, Sandro Queirós, Mustafa Anjari, Teresa Correia, Andrew P King, Anil A Bharath, Jack Lee

Abstract— **To date, regional atrial strains have not been imaged in vivo, despite their potential to provide useful clinical information. To address this gap, we present a novel CINE MRI protocol capable of imaging the entire left atrium at an isotropic 2-mm resolution in one single breath-hold. As proof of principle, we acquired data in 10 healthy volunteers and 2 cardiovascular patients using this technique. We also demonstrated how regional atrial strains can be estimated from this data following a manual segmentation of the left atrium using automatic image tracking techniques. The estimated principal strains vary smoothly across the left atrium and have a similar magnitude to estimates reported in the literature.**

I. Introduction

The upper chambers of the heart, the atria, play a crucial role in overall cardiac function, acting successively as a conduit, reservoir and booster pump for the blood entering the ventricles [1]. The link between atrial mechanical dysfunction and ventricular disease is well established, although it is not clear whether atrial functional deficits typically precede or are a consequence of ventricular pathologies such as left ventricular diastolic dysfunction [2].

Similarly, it is well known that atrial fibrillation (AF), the most common sustained cardiac arrhythmia, is also often accompanied by atrial mechanical dysfunction, although the mechanisms linking the two processes remain unclear [3]. Gaining a better understanding of these processes is likely to lead to an improvement in management and treatment for these patients. Catheter ablations, arguably the gold standard treatment for AF, have a single-procedure success rate below 50% in patient with long-standing forms of the disease [4]. The socio-economic burden of AF is thus immense, estimated as 1% of total healthcare costs in the UK [5].

The understanding of atrial mechanical function and its role in cardiac disease is greatly hampered by the lack of techniques capable of imaging atrial function at high resolution. So far, clinical value has been found in ratios of lengths of atrial segments (global atrial strains) typically measured using echocardiography. These have been found to be good predictors of, among others, post-ablation patient outcome [6], [7] and stroke risk [8] in AF.

Although dynamic magnetic resonance imaging (CINE MRI) has also been used to estimate global atrial function, these analyses have traditionally been based on one or two 8 to 10-mm thick 2D slices [9], [10]. This poor spatial coverage and resolution precludes an analysis of regional atrial strains, which are likely to be of important clinical value. In particular, abnormal regional strains may be an indicator of local substrate abnormalities, such as local fibrosis, given that fibrotic tissue is stiffer than healthy myocardium [11]. In fact, a positive correlation between global atrial strains and global atrial fibrotic burden has been reported [12], [13], but it is not clear whether this relationship would hold on a region by region basis. This is of high interest for two complementary reasons: it is increasingly believed that catheter ablation efficacy can be improved with personalized fibrosis maps [14]; and current MRI-based methods for fibrosis identification, which are based on late gadolinium enhancement, show poor reproducibility [15].

In this paper, we introduce a novel high-resolution CINE MRI acquisition protocol, capable of imaging the left atrium (LA) in one single breath hold (<25 s) at an isotropic acquisition resolution of 2 mm. We use this protocol to image the LA of 10 healthy volunteers and 2 cardiovascular patients over 20 phases of the cardiac cycle. We then create maps of principal strain values and principal strain directions for each subject across the cardiac cycle, as a proposed application for this novel technique.

II. Methods

A. Image Acquisition

We imaged 12 healthy volunteers (5 female, ages: 24-36 years old) and 2 cardiovascular patients (both male, ages: 32 and 54 years old) under ethical approval (IRAS ID: 171620). All subjects gave written informed consent prior to imaging.

*Research supported by the Wellcome/EPSRC Centre for Medical Engineering [WT203148/Z/16/Z], MedIAN EPSRC [EP/N026993/1] and the British Heart Foundation Centre of Research Excellence at Imperial College London [RE/18/4/34215].

M. Varela was with the School of Biomedical Engineering & Imaging Sciences, King's College London, UK. She is now with the National Heart and Lung Institute, Imperial College London, UK (corresponding author; e-mail: marta.varela@imperial.ac.uk).

S. Queirós is with the Life and Health Sciences Research Institute, University of Minho and the ICVS/3B's – PT Government Associate Laboratory, Braga, Portugal (e-mail: sandroqueiros@med.uminho.pt).

M. Anjari was with the Department of Radiology, Guy's and St Thomas' NHS Foundation Trust, London, UK. He is now with the Department of Neuroradiology, National Hospital for Neurology and Neurosurgery, University College London Hospitals NHS Foundation Trust, London, UK (e-mail: mustafa.anjari@nhs.net).

A. A. Bharath is with the Bioengineering Department, Imperial College London, UK (e-mail: a.bharath@imperial.ac.uk).

T. Correia, A. P. King and J. Lee are with the School of Biomedical Engineering & Imaging Sciences, King's College London, London, UK (e-mail: teresa.correia@kcl.ac.uk; andrew.king@kcl.ac.uk; jack.lee@kcl.ac.uk).

All images were acquired in a 1.5T Philips Ingenia MRI scanner, using a 32-channel cardiac coil, in a single breath-hold. Images were acquired in a short-axis view, planned with the help of traditional 2- and 4-chamber scans. A 3D bSSFP protocol (flip angle: 60°, TE/TR: 1.6/3.3 ms) was employed with SENSE (factor: 2.3-2.6) along both phase encode directions. Images were acquired with ECG-based retrospective gating in a typical field of view of 400 x 270 x 70 mm with an isotropic acquisition resolution of 2.0 mm and were reconstructed to 20 cardiac phases with 55% view sharing. The breath-hold duration depended on the heart rate of the imaged subjects and was kept under 25 s throughout. Images were reconstructed to a resolution of 0.6 x 0.6 x 1.0 mm for post-processing.

B. Image Analysis

Using the automatically detected R-wave of the vector electrocardiogram, we established the first cardiac phase, corresponding to end-ventricular diastole. The left atrial (LA) blood pool was manually segmented on the 10th cardiac phase by a medical expert. At this reference cardiac phase, the left atrium is round and close to its maximal volume.

The left atrial appendage and the insertion of the pulmonary veins were not included in the segmentation. Direct imaging of the atrial wall is not possible in this type of protocol, due to the thinness of the atrial wall (approx. 2.5 mm [16]), comparable to the acquisition resolution. Therefore, in contrast with ventricular deformation analyses, the atrial myocardium was therefore treated as an infinitesimally thin 2D surface embedded in a 3D space throughout.

For each short-axis slice which included the left atrium, the segmentation contour (corresponding to the LA endocardial wall) was approximated using cubic splines to obtain 150 evenly spaced control points. The position of each of these points in previous and subsequent cardiac phases was estimated, in 3D, using the Medical Image Tracking Toolbox, MITT [17]. Very briefly, MITT employs an iterative image tracking algorithm, called localized anatomical affine optical flow (AAOF), to estimate the motion and deformation of the object of interest across an image sequence. By using *a priori* knowledge of the object's shape to anatomically constrain the motion estimation, AAOF is able to iteratively propagate the segmented 3D surface to adjacent frames, and ultimately estimate the most likely position of each surface point across the entire cardiac cycle.

B. Regional Strain Calculation

The surface points in the reference frame were used to generate a smooth triangulated mesh using a radial basis function interpolation with regularization. This approach was implemented using Matlab (Mathworks, Natick, USA). It extrapolates beyond the upper and lower bounds of the image stack where no data points are available to produce a closed surface. Thereafter, the displacement fields between the reference frame and the rest of the time points were interpolated from the voxel grid onto the mesh to yield a series of deforming meshes.

The Lagrange strain tensor was estimated in the locally tangential surface plane using a finite element approximation and resolved into principal components at each node. The 2 principal components were sorted in descending order of magnitude. The trace and determinant of these strain tensors were also calculated. The normal component of the node-wise displacement vector was evaluated using the outward surface normal updated at each time point.

III. RESULTS

All acquired CINE MRI showed good contrast between the LA blood pool and adjacent structures and a very good signal to noise ratio. Figure 1 shows the acquired CINE MRI in the reference frame, in 3 orthogonal views for one healthy volunteer. The initial LA segmentation and corresponding mesh rendering are also shown.

The registered LA mesh for one of the imaged patients across three phases of the cardiac cycle is displayed in Figure 2, where the qualitatively good performance of the LA wall tracking algorithm can also be observed.

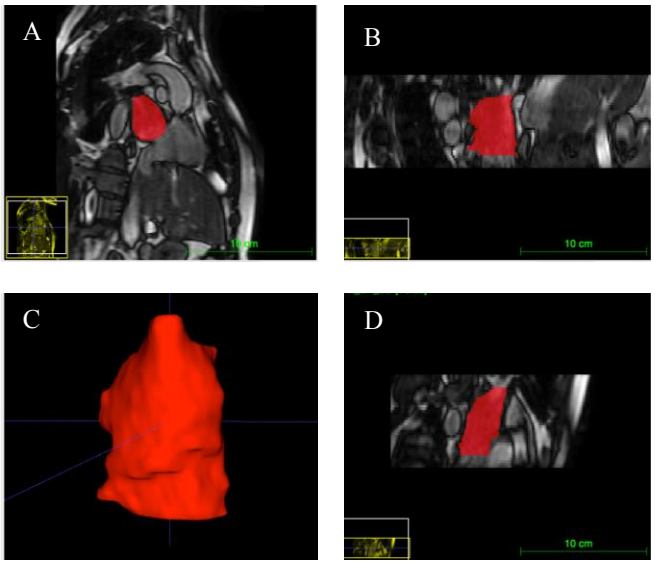

Figure 1 – Representative CINE MRI image (reference frame). Three orthogonal views (A, B, D) are shown overlaid with the manual left atrial segmentation and its rendering for a healthy volunteer (C).

The mesh generation yielded an average absolute distance error of 1.95±1.42 mm between the segmentation data points and the generated surface. In addition, the propagated meshes (as described in II. B) were compared to the results of direct mesh fitting to the data points at each frame (showed in Figure 2), which showed that the nodal discrepancies remained small (1.56±1.54 mm) except in regions of abrupt changes in curvature.

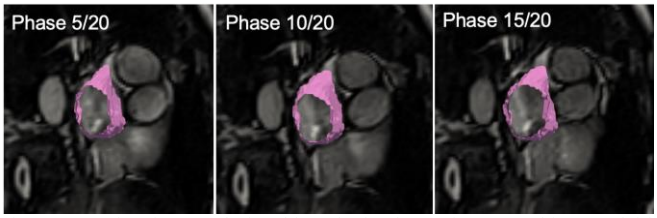

Figure 2 – Left atrium mesh (in white) obtained upon image tracking overlaid on the acquired CINE MRI in three different phases of the cardiac cycle (indicated in each subfigure), for one imaged patient.

Figures 3 and 4 show anterior and posterior views of the LA color-coded according to the value of the local principal strains for two representative subjects. Principal strain magnitude ranged between approximately ±0.5 across atrial regions and subjects. It was consistently higher close to the mitral valve and the roof of the atria and varied smoothly across the atrial surface.

Figures 3 and 4 also display vectors showing the direction of the principal strain vectors as arrows. Overall, principal strain directions varied smoothly both spatially and temporally. Some regions showed abrupt changes in principal strain direction, which could potentially be linked to the complex underlying atrial myofibre orientation [18].

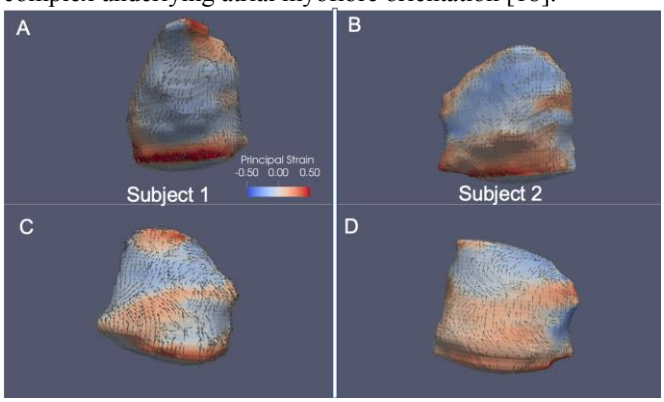

Figure 3 - Principal strains and strain vectors in the LA during **active atrial contraction** (phase 15/20) in two subjects. Panels A and B show anterior views, whereas panels C and D show posterior views of corresponding atria.

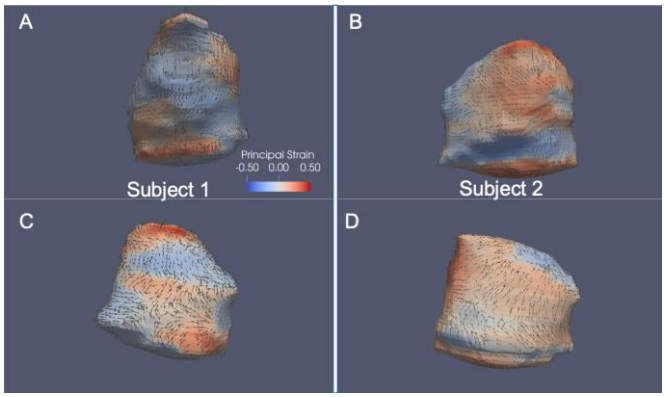

Figure 4 – Principal strains and strain vectors in the LA during **atrial reservoir function** (phase 5/20) in two subjects. Panels A and B show anterior views, whereas panels C and D show posterior views of corresponding atria.

Figure 5 shows a plot of LA volume across the cardiac cycle in a representative healthy volunteer. The reported volumes and ejection fraction are in agreement with literature from 2D CINE MRI [13] and 3D echocardiography [19]. The shape of the volumetric curve also agrees with published data [1], [19].

IV. Discussion

We present a novel protocol to acquire atrial CINE MRI in one single breath-hold at an isotropic resolution of 2 mm. Through the use of automatic tracking techniques, this protocol opens up the possibility of estimating regional atrial strains in 3D, which have been unexplored until now, despite their clinical interest.

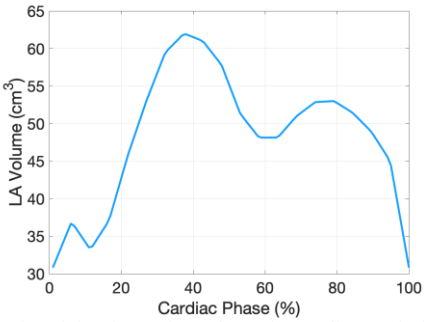

Figure 5 - Left atrial volume throughout the cardiac cycle in one healthy volunteer. The estimated LA ejection fraction, $EF = 100 \times \frac{(Vol_{Max} - Vol_{Min})}{Vol_{Max}}$, is 50.2%, where Vol_{Max} and Vol_{Min} are, respectively, the maximal and minimal LA volume across the cardiac cycle.

Given the lack of comparable imaging studies, it is difficult to validate our regional strain calculations. The good agreement of global metrics such as LA volumes (Figure 5) do provide some reassurance about the image processing pipeline, although the large spread of values in the literature [20] and the differences in methodology make direct comparisons difficult.

Of all the regional strain metrics obtained, we chose here to depict principal strain directions (interpretable as the direction of maximal local stretch) and principal strains (amount of stretch along that direction), as done before for the left ventricle [21]. The computed principal strains may not be directly comparable with the 2D strain metrics reported in echocardiography and 2D CINE MRI studies, as we are not limited to a single cross-sectional atrial view or to local surface area changes. It is nevertheless reassuring to note that the reported strain magnitudes in the literature (< 0.5) are qualitatively similar to what we observe in this study [7], [20].

It is expected that principal strains are, to a first approximation, aligned with regional average fiber orientation in the active atrial contraction phases of the cardiac cycle (Figure 3). During conduit and reservoir (Figure 4) function, the strains experienced by the atria are expected to depend more heavily on ventricular contraction and blood pressure. We did not, however, observe large changes in principal strain directions across time in most atrial regions.

V. Conclusion

We present a novel protocol to acquire atrial CINE MRI in one single breath-hold at an isotropic resolution of 2 mm. As a demonstration of the potential of this scan, we create regional atrial strain maps in 10 volunteers and 2 cardiovascular patients.

Future studies will provide further validation to the performed strain estimates through comparison with standard 2D LA strains estimated from 2-chamber and 4-chamber views. We will also investigate the potential clinical applications of this technique, for example, in aiding MRI-based identification of left atrial fibrosis and in predicting outcomes of atrial fibrillation patients.

References

[1] B. D. Hoit, "Left atrial size and function: role in prognosis.," *J. Am. Coll. Cardiol.*, vol. 63, no. 6, pp. 493–505, Feb. 2014.

[2] L. Thomas, T. H. Marwick, B. A. Popescu, E. Donal, and L. P. Badano, "Left Atrial Structure and Function, and Left Ventricular Diastolic Dysfunction: JACC State-of-the-Art Review," *Journal of the American College of Cardiology*. 2019.

[3] F. Bisbal, A. Baranchuk, E. Braunwald, A. Bayés de Luna, and A. Bayés-Genís, "Atrial Failure as a Clinical Entity: JACC Review Topic of the Week," *J. Am. Coll. Cardiol.*, vol. 75, no. 2, pp. 222–232, Jan. 2020.

[4] A. N. Ganesan *et al.*, "Long-term outcomes of catheter ablation of atrial fibrillation: a systematic review and meta-analysis.," *J. Am. Heart Assoc.*, vol. 2, no. 2, p. e004549, Apr. 2013.

[5] P. Kirchhof *et al.*, "2016 ESC Guidelines for the management of atrial fibrillation developed in collaboration with EACTS," *Eur. Heart J.*, vol. 37, no. 38, pp. 2893–2962, 2016.

[6] C. Schneider *et al.*, "Strain rate imaging for functional quantification of the left atrium: atrial deformation predicts the maintenance of sinus rhythm after catheter ablation of atrial fibrillation," *Eur. Heart J.*, vol. 29, no. 11, pp. 1397–1409, Jan. 2008.

[7] S. Montserrat *et al.*, "Left atrial deformation predicts success of first and second percutaneous atrial fibrillation ablation.," *Hear. Rhythm*, vol. 12, no. 1, pp. 11–18, Jan. 2015.

[8] J.-Y. Shih *et al.*, "Association of Decreased Left Atrial Strain and Strain Rate with Stroke in Chronic Atrial Fibrillation," *J. Am. Soc. Echocardiogr.*, vol. 24, no. 5, pp. 513–519, May 2011.

[9] M. Habibi *et al.*, "Cardiac Magnetic Resonance-Measured Left Atrial Volume and Function and Incident Atrial Fibrillation: Results From MESA (Multi-Ethnic Study of Atherosclerosis).," *Circ. Cardiovasc. Imaging*, vol. 9, no. 8, Aug. 2016.

[10] A. T. Huber *et al.*, "Cardiac MR Strain: A Noninvasive Biomarker of Fibrofatty Remodeling of the Left Atrial Myocardium," *Radiology*, vol. 286, no. 1, pp. 83–92, Jan. 2018.

[11] N. Zhang *et al.*, "Deep Learning for Diagnosis of Chronic Myocardial Infarction on Nonenhanced Cardiac Cine MRI," *Radiology*, vol. 291, no. 3, pp. 606–617, Jun. 2019.

[12] S. Kuppahally *et al.*, "Left Atrial Strain and Strain Rate in Patients With Paroxysmal and Persistent Atrial Fibrillation," *Circ. Cardiovasc. Imaging*, vol. 3, no. 3, 2010.

[13] M. Habibi *et al.*, "Association of left atrial function and left atrial enhancement in patients with atrial fibrillation cardiac magnetic resonance study," *Circ. Cardiovasc. Imaging*, vol. 8, no. 2, 2015.

[14] S. Nattel and D. Dobrev, "Controversies About Atrial Fibrillation Mechanisms," *Circ. Res.*, vol. 120, no. 9, pp. 1396–1399, 2017.

[15] R. J. Hunter *et al.*, "Diagnostic accuracy of cardiac magnetic resonance imaging in the detection and characterization of left atrial catheter ablation lesions: A multicenter experience," *J. Cardiovasc. Electrophysiol.*, vol. 24, no. 4, pp. 396–403, Apr. 2013.

[16] M. Varela *et al.*, "Novel MRI Technique Enables Non-Invasive Measurement of Atrial Wall Thickness.," *IEEE Trans. Med. Imaging*, vol. 36, no. 8, pp. 1607–1614, Aug. 2017.

[17] S. Queiros, P. Morais, D. Barbosa, J. C. Fonseca, J. L. Vilaca, and J. D'Hooge, "MITT: Medical Image Tracking Toolbox," *IEEE Trans. Med. Imaging*, vol. 37, no. 11, pp. 2547–2557, 2018.

[18] M. Varela, J. Zhao, and O. Aslanidi, "Determination of Atrial Myofibre Orientation Using Structure Tensor Analysis for Biophysical Modelling," in *Lecture Notes in Computer Science*, vol. 7945, S. Ourselin, D. Rueckert, and N. Smith, Eds. 2013, pp. 425–432.

[19] L. P. Badano *et al.*, "Standardization of left atrial, right ventricular, and right atrial deformation imaging using two-dimensional speckle tracking echocardiography: a consensus document of the EACVI/ASE/Industry Task Force to standardize deformation imaging," *Eur. Hear. J. - Cardiovasc. Imaging*, vol. 19, no. 6, pp. 591–600, Jun. 2018.

[20] B. D. Hoit, "Evaluation of Left Atrial Function : Current Status," *Struct. Hear.*, vol. 8706, no. 3–4, pp. 1–12, Jul. 2017.

[21] A. Satriano *et al.*, "Clinical feasibility and validation of 3D principal strain analysis from cine MRI: comparison to 2D strain by MRI and 3D speckle tracking echocardiography," *Int. J. Cardiovasc. Imaging*, vol. 33, no. 12, pp. 1979–1992, Dec. 2017.